AIAA SciTech Forum
23-27 January 2023, National Harbor, MD & Online
AIAA SCITECH 2023 Forum

10.2514/6.2023-0406

One-Dimensional Nitrogen based Resonantly Ionized Photoelectron Thermometry (N_2 RIPT)

Walker McCord[1], Aleksander Clark[2], and Zhili Zhang[3,*]
Dept. of Mechanical, Aerospace, and Biomedical Engineering, University of Tennessee, Knoxville, TN 37996, USA

A detailed calibration study of a non-intrusive, non-seeded one-dimensional (1D) rotational temperature measurement of molecular Nitrogen at atmospheric pressure is presented based on resonantly ionized and subsequent photoelectron induced fluorescence analysis for thermometry (N_2 RIPT). The RIPT signal is generated via directly probing various peaks within the resonant absorption band corresponding to the 3-photon transition $N_2\,(X^1\Sigma_g^+, v=0 \rightarrow b^1\Pi_u, v=6)$ near 285nm. This results in photoemission de-excitation that has significant fluorescence signal from the first negative band $N_2^+\,(B^2\Sigma_u^+ - X^2\Sigma_g^+)$. Discrete analysis of the fluorescence emissions found that the emission strength was directly related to the selected 3-photon transitional line strength ($T_{f,g}^3$) of the corresponding absorption band; enabling non-scanning two-wavelength thermometry. It is demonstrated that the technique is capable of generating RIPT signals of approximately 3 cm in length within a pure N_2 environment. Found wavelengths that are best suited for N_2 RIPT are tabulated and discussions on signal generation mechanism are discussed.

I. Nomenclature

J	=	the rotational quantum number
I	=	Laser Beam Intensity
k_B	=	Boltzmann Constant
E_g	=	Ground State Energy
N_0	=	Total number of N_2 molecules
$T_{f,g}^2$	=	two-photon transition line strength
λ_n	=	the excitation wavelengths for molecular nitrogen

II. Introduction

Non-intrusive thermometry techniques are ideal for probing gaseous systems where physical probes are prohibitive, as within high supersonic and hypersonic flight regimes that require minimal disturbances to the flow to maintain accuracy within regions of interest around test vehicles. Thermal gradients and heating play a critical role as significant aerodynamic heating occurring at high Mach numbers from reduced boundary layer heights and increased skin-friction dominates the design of test vehicles and their supporting aerothermal structures [1]. Weakening or failure of the thermal protection system or structure itself can lead to mission critical failures. While CFD simulations are ever increasing in fidelity and capacity, the complex fluid dynamics, dissociation, and real-gas

[1] Aeronautical Engineer, Senior, Lockheed Martin Aeronautics Company, Marietta, Georgia, AIAA Young Professional Member.
[2] Graduate Student, Dept. of Mechanical, Aerospace, and Biomedical Engineering, University of Tennessee, AIAA student member
[3] Professor, Dept. of Mechanical, Aerospace, and Biomedical Engineering, University of Tennessee, and AIAA Associate Fellow

effects often associated with hypersonic flight are still not fully understood [2]. The ability to experimentally and non-intrusively quantify thermal loads and heating imparted upon a vehicle is necessary to serve as validation for CFD simulations.

Some current non-intrusive optical thermometry techniques that exist include Planar-Laser Induced Fluorescence (PLIF), Tunable-Diode Laser Absorption Spectroscopy (TDLAS), and Coherent Anti-stokes Raman Scattering (CARS) [3]. PLIF must employ the use of a tracer molecule such as Nitric Oxide or an aromatic molecule, which can alter the flow chemistry and can result in nonreal flow features and behavior [4, 5]. TDLAS is path-integrated and limited to point measurements, making it difficult to isolate acquired data to within the test vehicle region [6-8]. There is a relatively new thermometry technique that utilizes Resonant Enhanced Multiphoton Ionization (REMPI) to ionize oxygen with sufficient energy to enable electron impacted excitation and subsequent ionization of local nitrogen molecules to produce sufficient photoemissions for thermometry applications; and is dubbed O_2 RIPT [9, 10]. The ionized nitrogen's main decay pathway is through photoemissions; the intensity of the emissions are directly related to the two-photon transitional line strengths of the corresponding excitation wavelength within the O_2 REMPI spectrum. By assigning a rotational state distribution analysis through fitting the captured signals to a Boltzmann distribution, vibrational gas temperature can be deduced. Additionally, the resonantly excited oxygen ionizes regions both pre and post focus of the laser allow for line thermometry measurements in approximately 3 cm have been reported [9]. This makes the newly developed technique an attractive option, but it suffers two inherent drawbacks; first it is a vibrational gas temperature measurement which in regions of non-equilibrium may never reach Local Thermodynamic Equilibrium (LTE) thus, the vibrational gas temperature may not be highly representative of the total gas temperature. Secondly, the technique relies upon oxygen molecules being present, ground test facilities can limit its applicability depending on the test gas being used.

The proposed technique build upon advances in O_2 RIPT, which has recently been demonstrated to achieve high spatial resolution of the vibrational O_2 temperatures through a supersonic under expanded jet [10]. N_2 RIPT differentiates from O_2 RIPT in that N_2 RIPT will directly resonantly ionize nitrogen for induced photoemissions; thus, it is relevant in either pure nitrogen or standard air mediums. O_2 RIPT works by resonantly ionizing oxygen molecules inducing electron impacted ionization of local nitrogen molecules, which mainly decay through photoemissions of the first negative band of nitrogen. The O_2 RIPT technique reliance upon the electron impacted excitation of N_2 means it is inherently constrained as a vibrational temperature measurement. N_2 RIPT fundamentally differs from O_2 RIPT in that by directly resonantly ionizing nitrogen molecules and using the photoemissions of the first negative band, the rotational states are directly probed thus, a 1D *rotational* gas temperature measurement is achieved. To achieve N2 RIPT, a focused frequency doubled dye laser tuned to energies of various rotational peaks within the $N_2(X^1\Sigma_g^+, v = 0 \rightarrow b^1\Pi_u, v = 6)$ absorption band are resonantly excited such that regions of high laser energy density is able to briefly populate locally available N_2 molecules to being N_2^+ via either a (3+1) or (3+2) REMPI scheme. The recombination of electrons and molecular nitrogen ions produces emissions of the first negative band of $N_2^+(B^2\Sigma_u^+ - X^2\Sigma_g^+)$ i.e.,

1. REMPI for molecular nitrogen, producing photoelectrons: $N_2^+(B) \rightarrow N_2^+(X) + h\nu_1$-
2. Further decay in the first positive band via: $N_2^+ + e^- \rightarrow N_2(B) \rightarrow N_2(A) + h\nu_1$+

The resulting emissions from the first negative band (Δv_0, 390nm; Δv_2, 425nm; Δv_1, 430nm) of N_2 are captured. Any light outside the band is removed via an optical bandpass filter. The signals are post-processed and the resulting values from the various bands are fed into a Boltzmann relationship that yields a 1D line temperature measurement with a nominal error of ±4%. In this paper, the establishment of technique is described in detail, providing future researchers the fundamental calibration studies of N_2 resonate peak sensitivities, suitable peaks for accurate measurements at various temperatures, and theoretical modeling of the N_2 (2+1) REMPI spectrum.

III. Experimental Setup

A general rendering for the calibration experiment for N_2 RIPT is shown in Fig. 1. The second harmonic of an Nd:YAG Laser (Continuum Surelite SL-10) with a pulse width of 8ns, repetition rate of 10 Hz, and 220mJ/pulse lasing energy was used to pump a dye laser (Continuum ND6000) that utilized a mixture of Rhodamine 590 and Rhodamine 610 to produce lasing light around 574nm (0.02 cm^{-1} linewidth). The dye laser was frequency doubled to

generate ultraviolet (UV) beam using an auto-tracker (Continuum UVT-1) to maintain a constant conversion efficiency from the frequency doubling crystal.

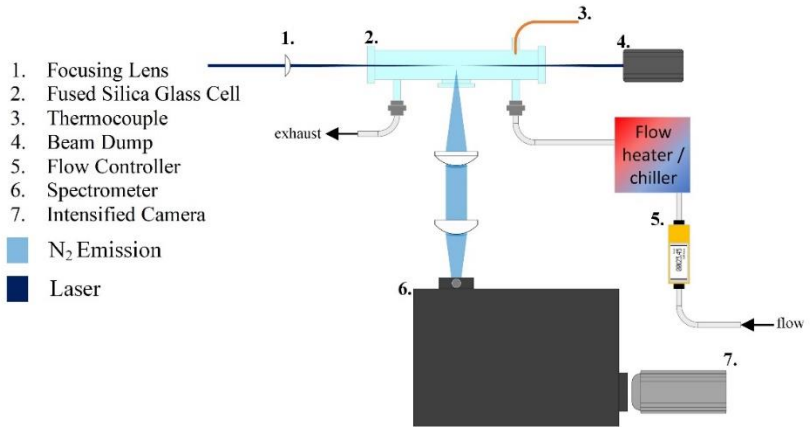

Figure 1: N_2 RIPT calibration experimental schematic.

The UV beam had energy of approximately 7.5 mJ/pulse from 284.5 to 286.0 nm. The UV beam was focused using a fused-silica spherical lens with focal length of +150mm, which generated a fluorescence line. The line was centered in a cylindrical, fused-silica glass cell. The emission spectra were collected via two +100mm spherical fused silica lenses that served to focus the light onto the slit of a spectrometer (Princeton Instruments, 600gr/mm blazed at 500nm) with a 60µm slit width. The spectrum was captured via an intensified scientific camera (PI-MAX4 1024f) with the sensor size of 1024x1024 pixels. To avoid local heating and maintain a uniform species number density in the area of interest, a constant flow of standard air was provided to the cell at a rate of 0-50 L/min via an electronic flow controller (OMEGA). Depending on the desired calibration temperature the air passed through either a flow heater (OMEGA) or through a custom-built flow-chiller to achieve temperatures ranging from 165 to 465 Kelvin and cell temperature was monitored by a K-type thermocouple and maintained within a tolerance of ±1% of the set point.

IV. Theoretical Discussions

A. RIPT from N_2 REMPI

In order to apply a state distribution analysis to assign temperature of N_2^+ photoemissions from N_2 REMPI; a rotationally resolved spectrum of N_2 must be obtained and the corresponding 3-photon transition cross-sectional data is needed to identify suitable peaks. A study of the REMPI structure of N_2 has already been conducted in detail in previous literature [11, 12]. For added coherency a brief summary is given. Both the ground state, $N_2(X^1\Sigma)$ and the excited state, $N_2(B^2\Pi)$ can both be described by Hund's case (a), in which hyperfine splitting is apparent in both the ground and excited states. For simplicity hyperfine structures apparent in the ground state will be denoted G_1, G_2, G_3, while hyperfine splitting in the excited state will be denoted F_1, F_2, and F_3. There is an adapted convention of adding subscripts of the hyperfine structures to the rotational branch, for example, Q_{14} represents the Q-branch which originates from G_4 and transits to F_1. For the nitrogen spectra resulting form 3-photon absorbance, the vibrational selection rules are governed by the Franck-Condon factor. Rotational selection rules dictate that seven rotational branches occur, given by table 1.

Table 1: Branches and allowed ΔJ cases.

Branch	ΔJ
N	-3
O	-2
P	-1
Q	0
R	1
S	2
T	3

The relative strengths of the individual ro-vibronic lines for the three-photon resonant transitions are calculated using Eq.1.

$$I_{calc} = Fg(J'')S(J',J'')exp\ (-E_{rot}/kT) \tag{1}$$

Were, F is the global factor that accounts for vibrational and electronic transition probabilities independent of the rotational transitions, g(J") is the nuclear spin statistical weight, S(J',J") is the multi-photon line strength factor, and $exp\ (-E_{rot}/kT)$, is the Boltzmann rotational populational distribution. Theoretical line strength factors, $S(J',J'')$, have previously been derived by Halpern [13] using coupled Schrödinger-equation calculations. The 3-photon factors include terms for the allowed ΔJ cases in Table 1, where the relative strength of the branches is dependent on the sum of the first and third order coupling terms. However, for the 3-photon resonant absorbance band $N_2(X^1\Sigma_g^+, v = 0 \rightarrow b^1\Pi_u, v = 6)$, only the P, Q, and R-branches contributed to the individual ro-vibronic lines. This indicates a dominance in of the first order coupling terms. Thus, the resulting line strength factors can be expressed by Eq. 2, Eq. 3, and Eq. 4. for the P, Q, and R-branches respectively.

$$S_P(J',J'') = \frac{1}{27}(J'' - 1) \tag{2}$$

$$S_Q(J',J'') = \frac{1}{27}(2J'' + 1) \tag{3}$$

$$S_R(J',J'') = \frac{1}{27}(J'' + 2) \tag{4}$$

Using the $S(J',J'')$ factors in Eq.2. Eq.3. and Eq.4., in Eq.1. a computational model that simulated the contributions from the P, Q, and R-branches within the $N_2(X^1\Sigma_g^+, v = 0 \rightarrow b^1\Pi_u, v = 6)$ absorption band. This model allows for identification of rotational peaks that could serve as potential candidates for direct excitation for providing the best fit of the resulting photoemissions to enable rotational temperature determination and is shown in Fig. 2. It should be noted, a similar model has been previously developed in literature exhibited high accuracy up to 600 Kelvin [14].

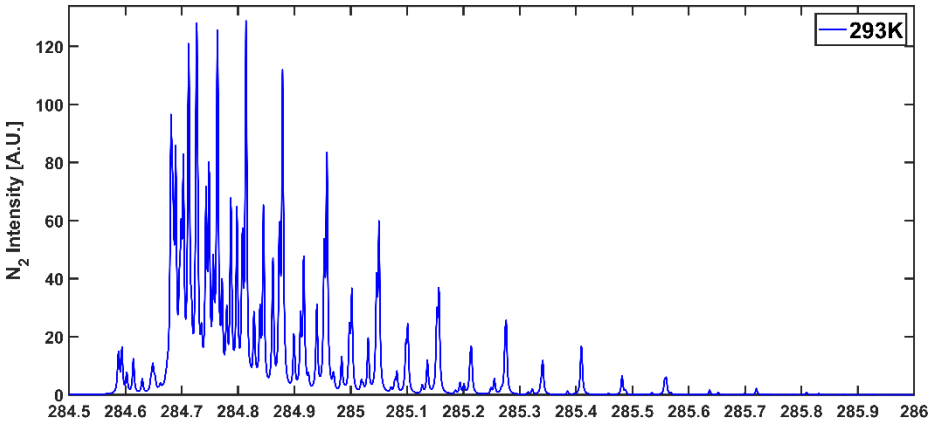

Figure 2: N_2 resonant absorption band corresponding to the 3-photon transition at 293 Kelvin.

Simulated absorption bands similar to Fig.2. were generated for a wide range of temperatures and then used to identify three-photon resonant peaks at various wavelengths that maintained sufficient population distributions and line strengths across the various thermal regimes. The resulting wavelengths that demonstrated high promise for yielding sufficiently high signal generation across all test point temperatures are tabulated in Table. 2.

Table 2: N_2 Selected Rotational Lines

λ_{laser} nm	branch	J'	G_1 cm^{-1}	$S(J',J'')$
284.712	Q(3),R(6)	3	1259.62	6.03
284.726	R(7),Q(4)	4	1215.67	6.91
284.748	Q(5),R(8)	5	1319.55	7.52
284.763	Q(6)	6	1259.62	9.99
284.787	Q(7)	7	1287.59	5.77
284.798	R(10)	10	1395.45	9.00
284.814	P(6)	8	1319.55	13.07
284.845	Q(9)	9	1355.50	7.30
284.862	R(12)	12	1487.29	10.49
284.879	Q(10)	10	1395.45	16.15
284.917	Q(11),P(9)	11	1439.38	8.84
284.940	R(14)	14	1595.09	11.98
284.958	Q(12)	12	1487.29	19.23
285.002	Q(13),P(11)	13	1539.20	10.38
285.031	R(16)	16	1718.80	13.47
285.050	Q(14),P(12)	14	1595.09	22.31
285.101	Q(15),P(13)	15	1654.95	11.92
285.157	Q(16),P(14)	16	1718.80	25.38
285.214	Q(17),P(15)	17	1786.63	13.46
285.276	Q(18),P(16)	18	1858.43	28.46
285.341	Q(19),P(17)	19	1934.21	15.00
285.409	P(18)	20	1858.43	12.63
285.482	Q(21)	21	2097.67	16.54
285.558	P(20)	22	2013.95	14.12

Using the values from Table.2, the theoretical resultant fluorescence from the two-photon transition from state g to f can be shown by Equ.1. By rearranging Eq.1. a more useful form given by Eq.5 can be had. Where the fluorescence from the selected peaks are termed I_{λ_n}, with n-subscript is typically termed 1 – 4 and denotes the specific wavelength fluorescence intensity. Typically it was found that the highest accurate fit that resulted in best temperature assignments were achieved with four peaks (wavelengths) used. Thus, four peaks will be selected for each air calibration temperature and a linear fit will be applied to the four signals that result equation 3, using those peak intensities. The resulting fit characteristics, such as R^2 and given temperature will determine which 4 peaks and resultant wavelengths are used.

$$Signal = \log\left(\frac{I_{\lambda_n}}{T^2_{f_n,g_n}}\right) \tag{5}$$

By taking the signal value from Eq.4 and applying a linear fit to the four selected signals, the slope of the fit will be used to approximate the local rotational temperature in the medium; which is given by Eq.6.

$$T_{fit} \propto {}^{1}/_{Signal \cdot k_B} \tag{6}$$

B. Calibration Experiments for N_2 RIPT

To identify specific rotational peaks most suitable for statistical fits of the Boltzmann plots, a calibration study was conducted at 165, 230, 293, 376, and 455 K in a gas cell. Ultra-purity Nitrogen was used as the working gas, and flown at a rate of 40 L/min to ensure the gas molecules in the cell ionized via N2 RIPT were evacuated and replaced between laser pulses. This was done to avoid localized heating and fluorescence saturation of the gas molecules. Additionally, all fluorescence signals collected were averaged over 200-images. This was to minimize shot-to-shot

laser fluctuations and background scattering artifacts. The use of a spectrometer allowed for discrete analysis of the first negative band emission of N_2^+, and each peak as well as the summation of the signals were studied for temperature dependence. Figure 3 shows a single shot raw image of generated N_2 RIPT signal via 284.748nm laser excitation with respective line average plot. The image was collected within the test environment at room pressure and temperature.

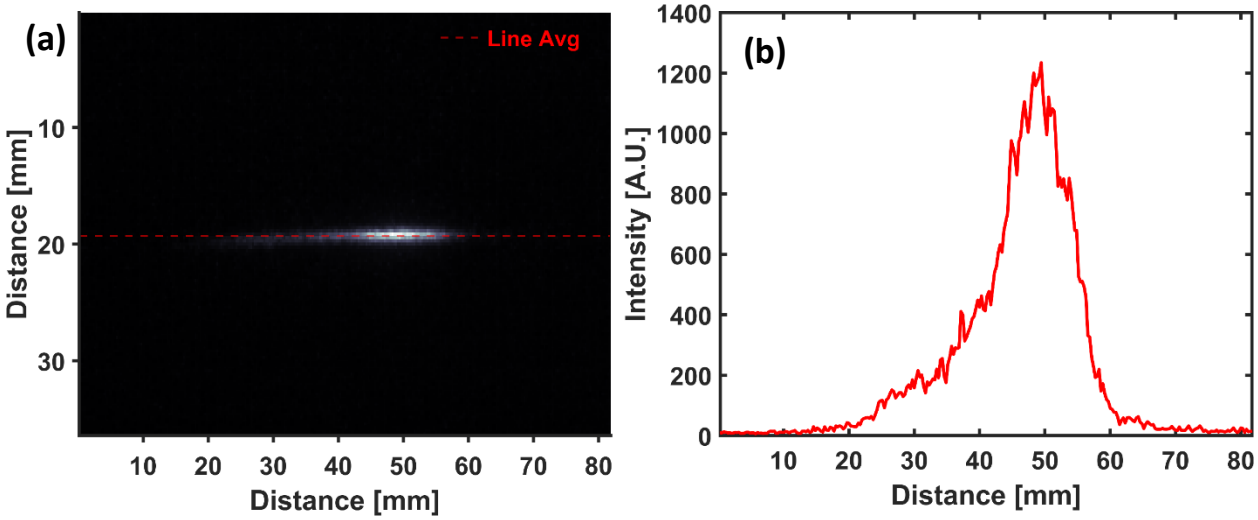

Figure 3: N_2 RIPT raw emission image (a), and line average (b).

For the calibration study, the image in Fig.3 was passed through a spectrometer, which was set to a center wavelength of 405nm allowing the ICCD to capture wavelengths between 370 to 440nm. This process was repeated for all wavelengths listed in Table 2 at the aforementioned temperature setpoints. To ensure high SNR and adequate spectrum resolutions, each image was background subtracted and collected with 200 accumulated on-chip exposures. The intensity value was found by integrating under each emission band for N_2. Care was taken to only include signal in the integration and excluding the background contribution. Signal values for 390, 425, and 430nm were studied and found that all emission peaks were capable of supporting N_2 RIPT. For further simplification, integration was performed under the full spectrum FOV. These were then processed using the aforementioned equations, from there 4 peaks were identified that resulted in the best fit; the results are shown in Fig.4.

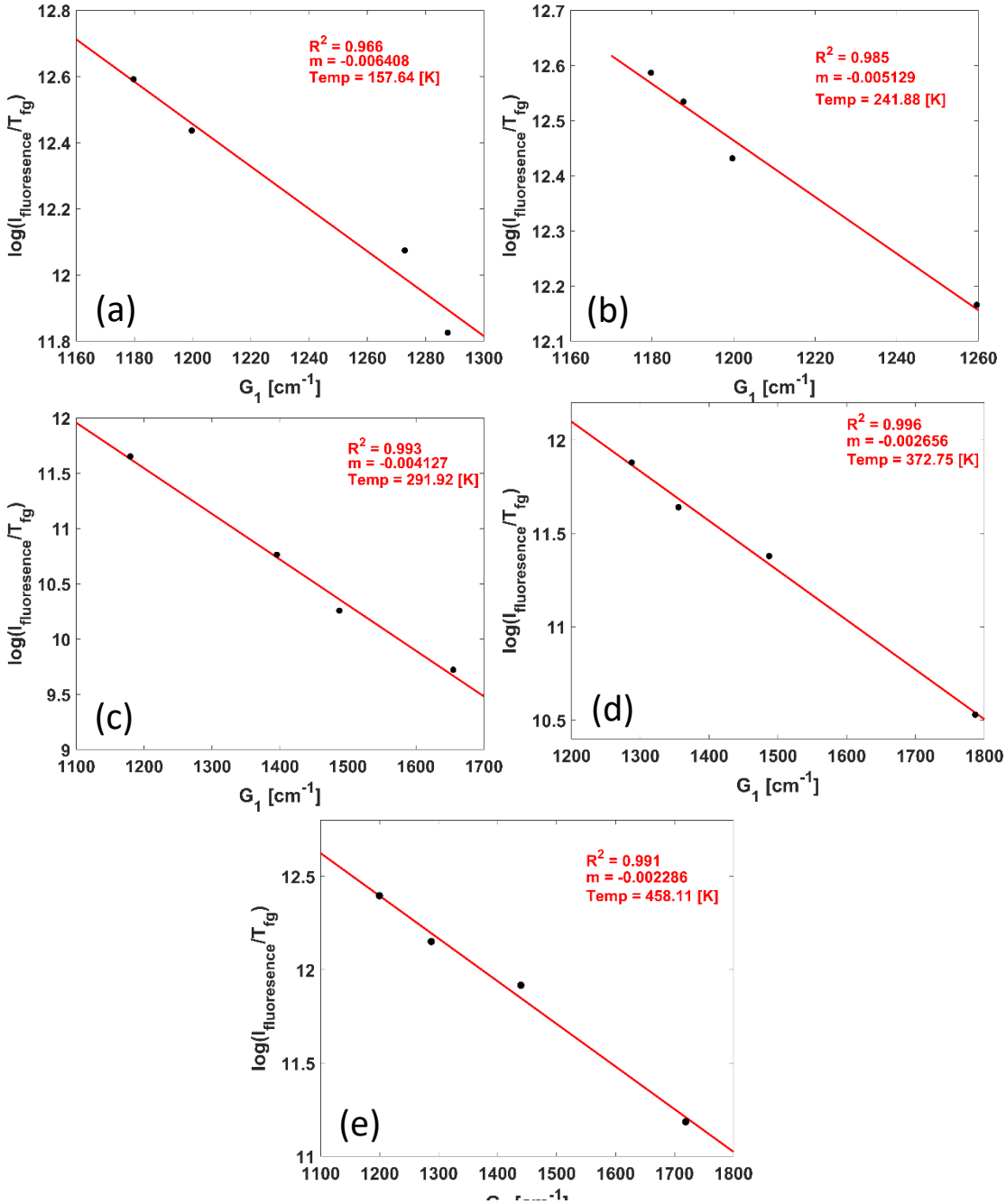

Figure 4: N_2 RIPT Temperatures fits for 165K (a), 230K (b), 293K (c), 376K (d), and 455K (e).

Figure 4 is the Boltzmann plot to determine the temperature sensitivities for various peaks. It indicates that through proper peak selection, N_2RIPT is capable of resolving temperature measurements with (±10K) accuracy. Peak selections, actual and predicted gas temperatures, and measurement error are detailed in Table 3. Based on equation (5) and (6), the x-axis of the Boltzmann plot is the energy of the rotational levels at the ground state, E_g from Table 1, and the y-axis is a log plot of the relative value of peaks in the experimental N_2RIPT spectrum scaled by the rotational line strength, ln $(I_{fluorescence}/T_{fg})$. Linear fitted lines are plotted for every measurement. At room temperature, the slope of the Boltzmann line gives a rotational temperature of 291K with an uncertainty of about 3%. At elevated temperatures, the Boltzmann plots give 458K for a furnace temperature of T_f = 455K with an uncertainty of 3%. Similar measurements show 157K for T_f = 165K and 241K for T_f = 230 K. The uncertainties are around 3-6%.

Table 3: Summary of N_2RIPT parameters for gas temperature assignments.

Identified Peaks				Act. Temp.	Meas. Temp	Error
nm	*nm*	*nm*	*nm*	*K*	*K*	*%*
284.712	284.748	284.763	284.814	165	157	4.85
284.712	284.726	284.748	284.798	230	242	5.22
284.712	284.879	284.940	285.031	293	292	0.34
284.814	284.862	284.940	285.101	376	373	0.80
284.748	284.814	284.917	285.050	455	458	0.66

Table 3 indicates that peak selection is critical for successful gas temperature determinations that are accurate. It is shown that the N_2RIPT generated signal is up to 30mm in length, thus enabling 1D nonintrusive thermometry measurements of critical distances within high-speed flow environments.

V. Conclusion

In this paper, a novel adaption to a relatively recent thermometry technique is proposed and validated through a detailed calibration study. By weakly ionizing a medium gas that contains nitrogen molecules, N_2RIPT utilizes resonant wavelengths to selectively excite N_2 rotational bands. Through multiphoton ionization processes, N_2 is weakly ionized producing spectra emissions within the $N_2^+(B^2\Sigma_u^+ - X^2\Sigma_g^+)$ emission band. Additionally, these emissions have been shown to be linearly dependent on temperature, albeit if the correct resonant peaks are used.

N_2RIPT is capable of resolving temperatures with an accuracy of ±4% and is capable of forming up to a 3 cm long line with the current setup used. The technique has two major advantages over the recently established O2RIPT. First, the fundamental mechanisms for signal generation enable N_2RIPT to bypass the inherent temporal limits that are associated with avalanche ionization. Thus, potential future work could focus on the technique's capacity for ultra-fast laser applications. Secondly, since pure nitrogen test gas is widely used in high-supersonic and hypersonic ground test facilities, to allow for reduced heating, this technique is high prevalent for future work in wind tunnel and CFD validation experiments. Currently, four shots are necessary to achieve an accurate and repeatable thermometry fit. Another avenue of future work will focus on expanding N_2 RIPT's capability, focusing on achieving thermal line profiles of an under expanded jet and boundary layer thermal gradient characterization on models in supersonic and hypersonic flow regimes.

VI.Acknowledgments

This work is supported by University of Tennessee, NSF- 2026242 and DOE.

VII. References

1. Lu, F. K. *Advanced hypersonic test facilities*: AIAA, 2002.
2. Cary, A. W., Chawner, J., Duque, E. P., Gropp, W., Kleb, W. L., Kolonay, R. M., Nielsen, E., and Smith, B. "Cfd vision 2030 road map: Progress and perspectives," *AIAA AVIATION 2021 FORUM*. 2021, p. 2726.
3. Childs, P. R., Greenwood, J., and Long, C. "Review of temperature measurement," *Review of scientific instruments* Vol. 71, No. 8, 2000, pp. 2959-2978.
4. Abram, C., Fond, B., and Beyrau, F. "Temperature measurement techniques for gas and liquid flows using thermographic phosphor tracer particles," *Progress in energy and combustion science* Vol. 64, 2018, pp. 93-156.
5. Lempert, W. R., Jiang, N., Sethuram, S., and Samimy, M. "Molecular tagging velocimetry measurements in supersonic microjets," *AIAA journal* Vol. 40, No. 6, 2002, pp. 1065-1070.
6. Chang, L. S., Strand, C. L., Jeffries, J. B., Hanson, R. K., Diskin, G. S., Gaffney, R. L., and Capriotti, D. P. "Supersonic mass-flux measurements via tunable diode laser absorption and nonuniform flow modeling," *AIAA journal* Vol. 49, No. 12, 2011, pp. 2783-2791.

7. Farooq, A., Jeffries, J. B., and Hanson, R. K. "In situ combustion measurements of H2O and temperature near 2.5 μm using tunable diode laser absorption," *Measurement Science and Technology* Vol. 19, No. 7, 2008, p. 075604.

8. Zhou, X., Liu, X., Jeffries, J. B., and Hanson, R. "Development of a sensor for temperature and water concentration in combustion gases using a single tunable diode laser," *Measurement Science and Technology* Vol. 14, No. 8, 2003, p. 1459.

9. McCord, W., Clark, A., and Zhang, Z. "One-dimensional air temperature measurements by air resonance enhanced multiphoton Ionization thermometry (ART)," *Optics Express* Vol. 30, No. 11, 2022, pp. 18539-18551.

10. McCord, W., Gragston, M., Plemmons, D., and Zhang, Z. "O 2 based resonantly ionized photoemission thermometry analysis of supersonic flows," *Optics Express* Vol. 30, No. 22, 2022, pp. 40557-40568.

11. Adams, S., and Williamson, J. "Gas temperature measurement in atmospheric nitrogen discharge by laser REMPI-LIF technique," *Bulletin of the American Physical Society* Vol. 55, 2010.

12. McGuire, S., and Miles, R. "Collision induced ultraviolet structure in nitrogen radar REMPI spectra," *The Journal of Chemical Physics* Vol. 141, No. 24, 2014, p. 244301.

13. Halpern, J., Zacharias, H., and Wallenstein, R. "Rotational line strengths in two-and three-photon transitions in diatomic molecules," *Journal of Molecular Spectroscopy* Vol. 79, No. 1, 1980, pp. 1-30.

14. Adams, S. F., Williamson, J. M., and Fisher, D. M. "Rotational temperature analysis of N2 by resonant enhanced multi-photon ionization with fluorescence detection," *Journal of Applied Physics* Vol. 110, No. 8, 2011, p. 083309.